Journal of Cranio-Maxillo-Facial Surgery 47 (2019) 293–299

Contents lists available at ScienceDirect

Journal of Cranio-Maxillo-Facial Surgery

journal homepage: www.jcmfs.com

Computer-assisted surgery for reconstruction of complex mandibular defects using osteomyocutaneous microvascular fibular free flaps: Use of a skin paddle-outlining guide for soft-tissue reconstruction. A technical report

Salvatore Battaglia [a], Francesco Ricotta [a], Vincenzo Maiolo [c], Gabriella Savastio [c], Federico Contedini [b], Riccardo Cipriani [b], Barbara Bortolani [d], Laura Cercenelli [d], Emanuela Marcelli [d], Claudio Marchetti [a], Achille Tarsitano [a, *]

[a] Maxillofacial Surgery Unit, S. Orsola-Malpighi Hospital, Department of Biomedical and Neuromotor Sciences, (Head Prof. Claudio Marchetti), Alma Mater Studiorum University of Bologna, Bologna, Italy
[b] Plastic and Reconstructive Surgery Unit, (Head Dr. Riccardo Cipriani), Policlinico S. Orsola, Bologna, Italy
[c] Radiology Department, (Head Prof. Alessio Giuseppe Morganti), S. Orsola-Malpighi Hospital, Alma Mater Studiorum University of Bologna, Italy
[d] Department of Experimental, Diagnostic and Specialty Medicine, Bioengineering Laboratory (Head Prof. Emanuela Marcelli), S. Orsola-Malpighi Hospital, University of Bologna, Italy

ARTICLE INFO

Article history:
Paper received 10 July 2018
Accepted 20 November 2018
Available online 28 November 2018

Keywords:
CAD/CAM
Fibular free flap
Mandibular reconstruction
Virtual planning
Computed topographic angiography
Computer-assisted surgery

ABSTRACT

Introduction: We present our pre-operative virtual planning of complex mandibular reconstruction with a microvascular fibular composite free flap and its harvesting using our novel cutaneous positioning guide based on the perforator vessels for our soft tissue reconstructive surgery.
Technical report: We applied our protocol to 42 consecutive patients needing mandibular composite reconstruction. All patients were preoperatively studied with a CTA scan to evaluate the fibular pattern of vascularization and the perforator vessels three-dimensional path and position. Computer assisted surgery (CAS) was performed: a skin paddle outlining guide (SPOG) was designed to reproduce the shape and area of the planned soft tissue resection. CTA measurements and in vivo findings were compared. After performing the CTA, we classified the viable perforators in High Perforators, Medium Perforators and Low Perforators. The average diameter of the perforator vessels was 3 mm. The average difference between the measurements performed on the CTA and the intra-operative measures was 1, 4 mm.

The SPOG was based on calf proximal and distal diameters. The anatomical fitting of the guide was obtained thanks to two customized flanges that embrace circumferentially the proximal and distal portions of the leg.

The SPOG encompassed appropriate skin/leg regions, allowing the surgeon to localise the required perforator vessel.
Conclusions: CTA protocol appears to be a valuable approach to asses and virtually simulate composite mandibular reconstructions. The SPOG seems to be a valuable tool to reproduce intra-operatively the planned soft tissue area to be reconstructed.

1. Introduction

Reconstruction of complex three-dimensional (3D) mandibular defects challenges head-and-neck surgeons (Cordeiro et al., 1999), who must meet morphological and anatomical goals and optimise patient quality-of-life and functional outcomes. The general consensus is that the reconstructive gold standard in such

* Corresponding author. Maxillofacial Surgery Unit, S.Orsola-Malpighi Hospital, Department of Biomedical and Neuromotor Sciences, Alma Mater Studiorum University of Bologna, Via G. Massarenti 9, 40100 Bologna, Italy.
E-mail address: achille.tarsitano2@unibo.it (A. Tarsitano).

https://doi.org/10.1016/j.jcms.2018.11.018
1010-5182/

situations is a microvascular composite fibular free flap (Kumar et al., 2016).

The use of computer-aided design/computer-aided manufacturing (CAD/CAM) prior to mandibular reconstruction is now essential (Tarsitano et al., 2014), as it allows accurate planning and affords excellent surgical outcomes (Tarsitano et al., 2015). This especially true when complex 3D defects are apparent; it remains very challenging to ensure appropriate soft-tissue positioning during composite microvascular free flap reconstruction. Moreover, osteomyocutaneous fibular flap harvesting per se may need to be modified intra-operatively when planning is inadequate, an aberrant anatomy is encountered, or the perforator vessels are not viable to support transferred skin paddle. In such cases, it may be necessary to explore the contralateral leg or harvest a different flap (Garvey et al., 2012). Previously, we developed a computed tomography angiogram (CTA) protocol to preoperatively assess leg vascular anatomy, the perforator vessels, and spatial localization and disposition (Battaglia et al., 2017).

Building on this, we here present a technical report based on our protocol for complex mandibular reconstruction using a microvascular fibular composite free flap and flap harvesting using CAD/CAM, fibular cutting guides, and a novel cutaneous positioning guide derived by reference to the perforator vessels chosen for soft-tissue reconstructive surgery.

2. Material and methods

We applied our technical protocol on 42 consecutive patients (21 males and 21 females) of an average age of 51.4 years (range 11–82 years). The average follow-up period was 14.9 months (range 1–30 months).

The study was approved by our local Ethics Committee (no: 62/Sper/AOUBo).

2.1. Resection Planning

The resection planning included detailed bone information as well as other tumour characteristics such as localisation, size, shape and extension according to other previously published models (Kraeima et al., 2015, 2018). It is best to extract this information from multi-modality imaging: CT and MRI together because the individual information is not enough. Information as provided by CTs and MRIs is crucial for adequate resection planning.

Each patient was preoperatively assessed by high-resolution CT (1, 25-mm-thick sections, 0, 625-mm reconstruction) of the head and neck, with and without contrast enhancement, and magnetic resonance with gadolinium.

Clinical observations and pre-operative imaging derived tumour information were only combined with the virtual plan through the radiologist and surgeon's interpretation. A 3D virtual model of both the mandible and surrounding tissues is thereby available for careful inspection and detailed resection margin planning (Fig. 1).

Determination of tumour volume and oncologic margins is obtained and surgical margins were recorded according to our institutional guidelines (at least a 10 mm tumour-free margin).

2.2. CTA of the leg

All CTA scans were obtained by the same radiologist using the same image-acquisition protocol. We used a 64-slice multi-detector CT scanner (Lightspeed VCT LS Advantage, General Electric Medical Systems); the parameters were 120 kV, maximum 300 mA, pitch 0.5, rotation time 0.8 s, table speed 40 mm/rotation, slice thickness 0.6 mm, collimation 0.6 mm, and matrix size 512 × 512. Initial scouting images were acquired to determine scan volumes. All scans proceeded in the antegrade direction (both legs simultaneously) from above the knee to the foot. We scheduled baseline non-contrast acquisition and arterial-phase scanning for all cases; venous phase scans (after 60 s of delay) were acquired for a few patients exhibiting flow delays or changes. We employed the bolus tracking technique; we identified when contrast medium filled the leg vessels of interest. Scanning commenced when the enhancement peak appeared. Each region of interest (ROI) in terms of vessel filling was fixed at a particular point, generally in the distal, superficial femoral artery or the proximal popliteal artery; the ROI was centred within the artery of choice and sized to include only the arterial lumen. A non-ionic contrast medium (350 mg iodine/mL; Xenetix 350 Guerbet or Iomeron 350 Bracco; volume 100–120 mL) was power-injected at a maximal flow rate of 4.5 or 5.0 mL/s into an antecubital vein via a 20-gauge needle, and CTA typically lasted 40 s. The amount of contrast medium injected depended on examination duration and flow rate. Multi-planar 3D reconstructions (maximum intensity projections [MIPs] and volume-rendered (VR) reconstructions) were created. Various post-processing techniques facilitated the interpretation of axial images, identification of fine vessels, and measurement of pedicle lengths and diameters.

2.3. CAD-CAM protocol

The CAD/CAM protocol commenced with processing of Digital Imaging and Communications in Medicine (DICOM) files from head-and-neck CT and donor-site CTA using MIMICS software (Materialise, Leuven, Belgium) to obtain virtual 3D models allowing surgical planning, including radical resection of malignancies.

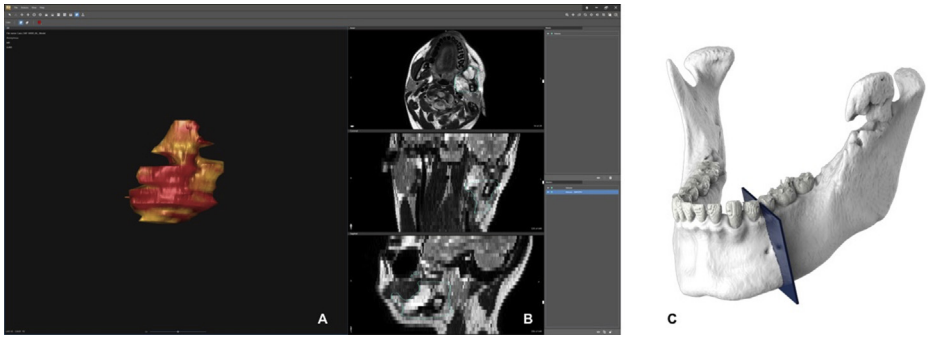

Fig. 1. Example of the planned volume for tumour resection obtained using the D2P™ software (3D Systems) on pre-operative MRI (A, B) and CT scan (C). A: Segmented tumour volume; B: Tumour borders definition on MRI; C: Bone resection planning on 3D model from patient CT scan.

Fig. 2. The resected soft-tissue surface is outlined during resection planning (A) and transferred, with the correct shape and area, to the skin of the 3D virtual donor leg model (B).

For unilateral defects, a mirroring function was used to ensure a symmetrical anatomical outcome. When secondary reconstructions were planned, we sought to maximally restore the original anatomy by reference to the CT scan of the native mandible, when available or otherwise, using a library mandible affording optimal dental occlusion. As for resection, we simulated reconstruction using the 3D DICOM rendering of the donor site. The customized reconstructive titanium plate that would support the fibular osteomyocutaneous free flap was designed by thickening the outer surface of the healthy side of the mandible. In this way, it was possible to obtain an ideal aesthetic contour and avoid bone deformities. Each plate was fixed to the native mandible using the 2.4 locking system. This phase of planning was performed by surgeons (aided by a dedicated engineer) using Geomagic Freeform-Plus software (3D Systems, Rock Hill, South Carolina, USA). Resection cutting guides and osteotomy guides for bony free flaps were planned with the aid of TRIMATIC software (Materialise). The virtual planning files were validated by the surgeons and verified with the aid of MAGICS software (Materialise). Solid-to-layer (STL) files were then used for plate manufacture (Sintac srl, Trento, Italy) via direct metal laser sintering (DMLS M280 system; Electro-Optical Systems GmbH, Krailling, Germany) layer by layer (Leiggener et al., 2009). Similarly, the STL files of the cutting and osteotomy guides were printed using the SLS FORMIGA P110 system (Electro-Optical Systems GmbH). We also designed customised cutting guides for bony free flaps to allow for precise osseous segmentation. Each osteotomy cutting guide considered the position of the perforator vessel to be used in soft-tissue reconstruction. We estimated the surface of the estimated soft tissues resection and we outlined this surface on the skin of the 3D donor leg model (Fig. 2); customised cutting guides based on calf proximal and distal diameters were then created. The anatomical fitting of the guide on patient's calf is obtained thanks to the shape of guide itself: two customized flanges embrace circumferentially the proximal and distal portions of the leg.

In addition, the skin paddle outline guides (SPOGs) encompassed appropriate skin/leg regions, allowing the surgeon to localise the required perforator vessel (Fig. 3).

The reconstructive flap was then virtually transferred to its ultimate position, together with soft tissue (Fig. 4). Moreover, we ensured that the pedicle length was always adequate to allow the flap to attain the neck vessels to be used for microvascular anastomosis.

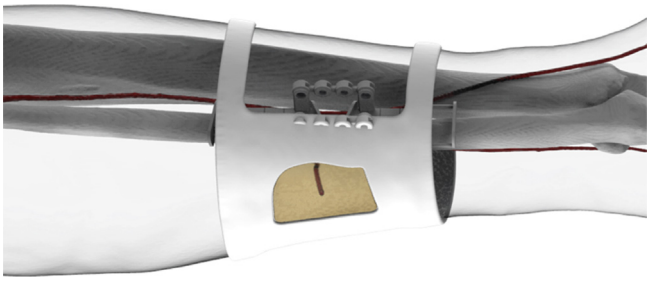

Fig. 3. Design of the skin paddle-outlining guide (SPOG). The desired shape is outlined on the skin of the leg model, and the guide is then designed by reference to the calf proximal and distal diameters.

Fig. 4. Virtual placement of the osteomyocutaneous microvascular fibular free flap supported by a customised reconstructive plate. The soft tissue is virtually positioned in the final setting.

2.4. Surgical technique

To intraoperatively reproduce the planned resection, mandibular cutting guides (additively printed in polyamide) were positioned as virtually planned. All patients underwent reconstructions using osteomyocutaneous microvascular fibular free flaps. Flap harvesting commenced with marking of the fibular head and the lateral malleolus and then by connecting these points with dots drawn on the skin. The skin paddle shape and position (centred on the CTA-identified perforator vessel) was also marked on the skin using the SPOG device as preoperatively planned (Fig. 5). This customised skin cutting guide was based on calf proximal and distal

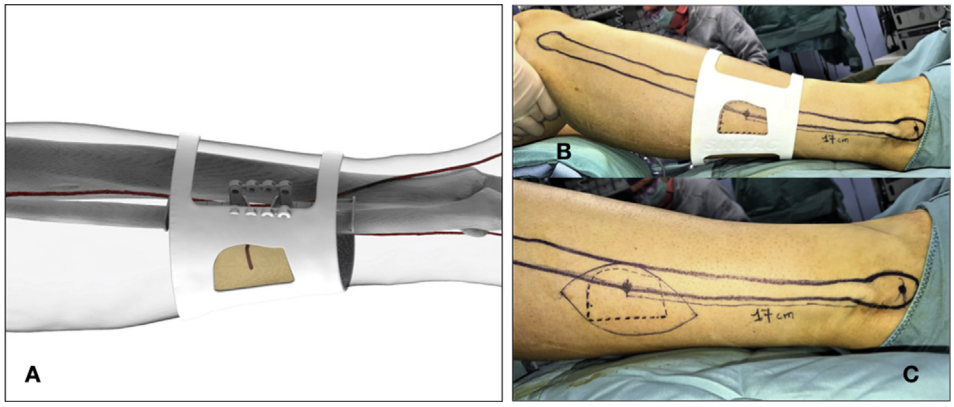

Fig. 5. Intraoperative use of the SPOG. A: Virtual planning of the skin paddle and SPOG design. B: Intraoperative positioning of the SPOG; a good fit to the calf is apparent. C: Outlining the shape of the skin paddle required for reconstruction.

diameters. The anatomical fitting of the guide on patient's calf is obtained thanks to the shape of guide itself: two customized flanges embrace circumferentially the proximal and distal portions of the leg. In addition, the SPOGs encompassed appropriate skin/leg regions, allowing the surgeon to localise the required perforator vessel. After outlining the skin paddle shape and surface using the SPOG, the guide was removed and an incision was created over the posterior intermuscular septum along a previously marked line. The skin was then incised as dictated by the SPOG, anteriorly over the peroneus muscle, approximately 2 cm above the lateral malleolus, and over the fibula. The guide allowed the surgeon to position the skin paddle exactly as pre-planned. Harvesting then proceeded along the posterior intermuscular septum; the common peroneal nerve was located and preserved below the head of the fibula. On anterior elevation of the skin paddle, the perforator was identified, and the accuracy of preoperative localisation double-checked as described above (Video 1). After incision of the anterior intermuscular septum and dissection of the extensor digitorum and hallucis longus muscles, the fibula was identified and bluntly dissected. The fibular cutting guide was then positioned, as pre-planned, centred on the perforator vessel of the skin paddle. The guide was fixed to the fibula using 2.0 mono-cortical screws. Proximal and distal osteotomies were performed on the opposite side of the pedicle using an oscillating saw. The peroneal artery and vein were identified, ligated, cut distally, and the flap was then detached. The cutting guide allowed accurate bone segmentation, as pre-planned. Also, the holes in the fibular cutting guides were in the same locations as those of the reconstructive plates, allowing the surgeon to correctly and rapidly place bony segments during reconstruction.

Supplementary video related to this article can be found at https://doi.org/10.1016/j.jcms.2018.11.018.

3. Results

3.1. CTA donor site evaluation and perforator vessels accuracy assessment

CTA was used to reveal all major arteries of the calf and foot, including the popliteal, anterior tibial, posterior tibial, peroneal, and dorsalis pedis arteries. The dominant and patent arterial supply to the pedal arch was identified. All images were reviewed in terms of arterial abnormalities (stenosis or occlusion) and/or aberrant anatomy. Any anomaly (any earlier fracture; a benign or malignant lesion; and/or soft tissue, muscular, or subcutaneous change) was reported.

CTA was used to locate all viable perforator vessels, their sources on the peroneal artery (Fig. 6A), and to measure the distances between its subcutaneous projection and the middle point of the head of the fibula and of the external malleolus (Fig. 6B).

The anatomical distribution of viable perforator vessels in 84 legs studied via CTA was identified and reported on a coronal leg reconstruction. The perforator vessels distribution was classified into three categories in relation to the distance from the external malleolus: low perforators (between 10 and 15 cm), medium perforators (between 15 and 20 cm), high perforators (between 20 and 25 cm). The pattern of distribution revealed three peaks. For the right legs, a rate of 42% of perforator vessels was classified as low perforators (LPs); a rate of 23% as medium perforators (MPs); a rate of 35% as high perforators (HPs). For the left legs, rates of 44%, 29%, 27% were reported for LPs, MPs, and HPs respectively (Fig. 7).

3.2. Accuracy of the transfer of the virtual planning to the clinical situation

Accuracy of the transfer of the virtual planning to the clinical situation was evaluated as the correspondence between pre-operative planning and post-operative CT-scan. It reflects the reproducibility of the planning thanks to the cutting guides realized based on CTA. The STL files used for virtual planning and the STL files of the post-operative CT scan were imported into an open source mesh processing software tool (MeshLab; Visual Computing Lab, ISTI-CNR, Pisa Italy). The two meshes obtained were first aligned taking into consideration fixed reference landmarks on the virtual planning and postoperative CT scan (such as the screw holes on the plate or plate surface) to obtain the most accurate three-dimensional overlap. The software automatically overlapped the STL files based on these parameters.

Once the overlapping was complete, the accuracy of the reconstruction was assessed using the automated Hausdorff distance function of the software, setting the postoperative mesh as the target mesh (Fig. 8).

In this way, it was possible to calculate the minimum, maximum, and average error for each reconstruction as the difference between post-operative mesh and virtual planning, exactly in the same way and with the same settings.

The data were registered using Microsoft Excel 2013 (Microsoft Corp., Redmond, WA, USA). The average minimum error, the average maximum error, and the average mean error were calculated for our series of mandibular reconstructions.

The average mean error for the bony reconstruction was 1 mm (range 0.4–2.46 mm).

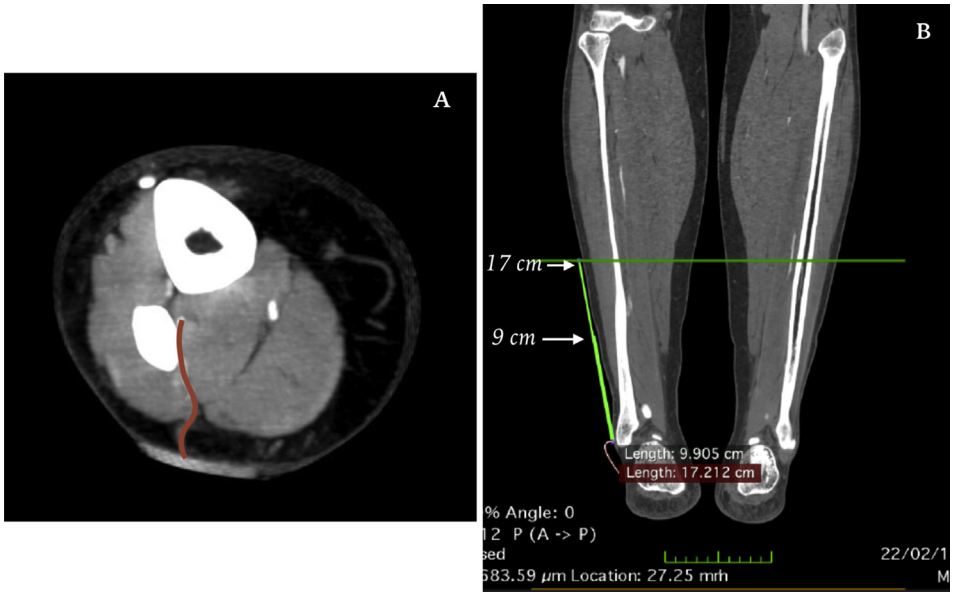

Fig. 6. Perforator vessels localization on CTA. A: perforator source from the peroneal artery and its path to the subcutaneous tissues visualized on axial plane. B: assessment of the distances between perforator vessel subcutaneous projection and the middle point of the head of the fibula and of the external malleolus, visualized on coronal plane.

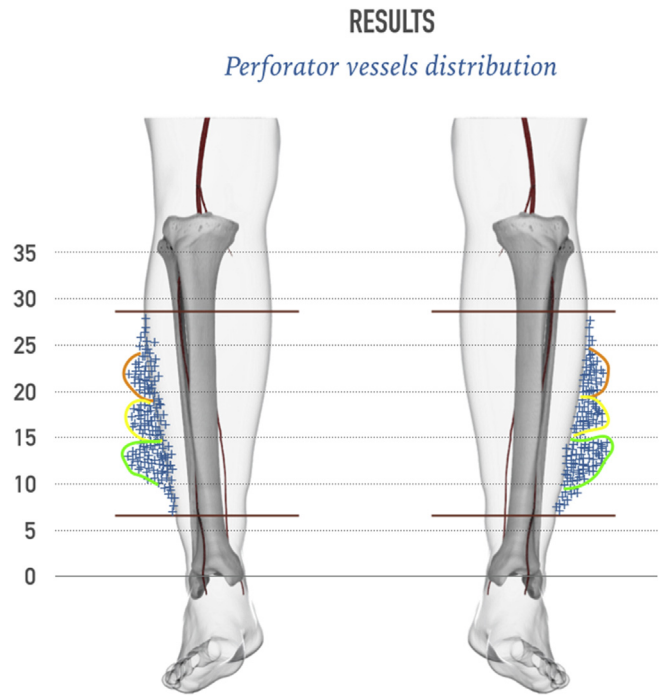

Fig. 7. Quantitative distributions of viable perforator vessels in 84 legs studied via CTA. Three peaks are evident: high perforators (HPs; orange), medium perforators (MPs; yellow), and low perforators (LPs; green).

3.3. Surgical reconstructive outcomes

Reconstructive outcomes were evaluated as donor site and flap complications. Time needed for flap segmentation and insetting was registered. The start-off time point was defined as the moment when reconstruction could begin (when the osteotomies were performed on the raised fibula). The endpoint was when the reconstruction plate was screwed to the proximal segments of the mandible and the fibular skin paddle was in place.

We harvested 36 osteomyocutaneous microvascular fibular free flaps. We encountered no intra-operative pedicle damage. No contralateral leg exploration was needed. No additional microvascular salvage flap was harvested. No perforator vessel was damaged during skin paddle harvesting. No postoperative donor site complication was encountered.

The mean reconstructive time (time needed for flap segmentation and insetting) was 36.5 (range, 23–45) min. When the mean reconstructive time was broken down to time per segment, a fibular segment took 10 min.

4. Discussion

Reconstruction of 3D complex mandibular defects remains very challenging; the mandible is critical in terms of aesthetics, social interactions, and functionality (Kumar et al., 2016). CAD/CAM mandibular reconstruction has improved planning, precision, and the operative time (Wilde et al., 2015; Tarsitano et al., 2018). The 3D additive printing of cutting guides and reconstructive plates has greatly improved surgical outcomes (Tarsitano et al., 2014). Although planning software is constantly updated, soft-tissue simulation remains imprecise. It is difficult to assess the required size of the skin paddle to be harvested with the fibular free flap. Also, poor planning, an aberrant anatomy, and an inadequate soft-tissue perforator vessel may force exploration of the contralateral leg or the choice of a different flap (Garvey et al., 2012). Many imaging techniques (e.g. traditional angiography) have been used in efforts to reduce donor site complications. As CTA is highly accurate and non-invasive, CTA is now the gold standard for pre-operative lower leg assessment (Ribuffo et al., 2010). Other imaging protocols more accurately reveal the soft tissues of the leg, but they do so less reliably for bone, rendering additional imaging assessments necessary (Hölzle et al., 2011).

We recently assessed the accuracy of our CTA protocol in terms of anatomical vascular variations in donor legs and, particularly, in terms of visualisation of cutaneous perforators of the peroneal artery (Battaglia et al., 2017). We 3D-rendered the perforator vessels using appropriate thresholding; we created osteotomy guides reflecting the chosen perforators, reducing the risk of vascular damage during skin paddle harvesting. Here, we (prospectively) found that our CAD/CAM workflow also aided in skin

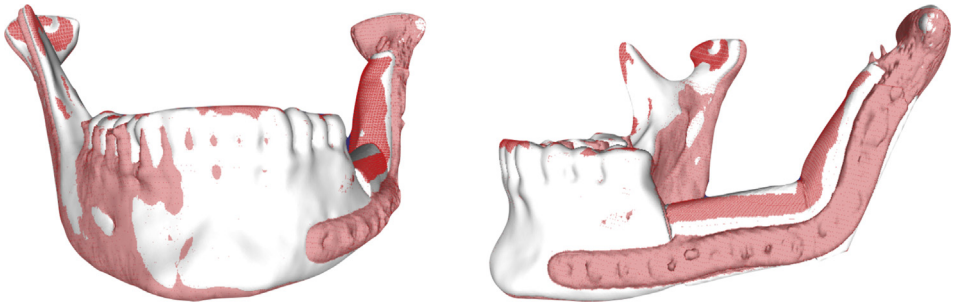

Fig. 8. Superimposition between virtual surgical planning (white colour) and post-operative CT (red colour) in frontal and lateral view. The accuracy of the reconstruction was assessed using the automated Hausdorff distance function of the software, setting the postoperative mesh as the target mesh.

paddle planning. During this workflow, we simulated cutaneous or intra-oral extensions of soft tissue defects, transferred these to 3D leg models in terms of the required contours, and designed SPOGs by reference to the chosen perforator vessels; the SPOGs reflected the required paddle shapes and contouring. Thus, we reduced the accidental perforator damage associated with post-detachment flap remodelling. Moreover, flap placement time was reduced and it was unnecessary to perform significant adjustment of paddle shape, with respect to the SPOG design. Regarding flap segmentation and insetting time, data obtained from our series confirm the results previously published in 2016 (Tarsitano et al., 2016). Indeed, fibular cutting guide and SPOG have the potential not only to reduce surgical time but also to reduce ischaemic time for the fibular flap. This was clearly demonstrated in the present study by the fact that the mean reconstructive time (time needed for flap segmentation and insetting) was 36.5 (range, 23–45) min. Differently, the mean reconstructive time for freehand reconstructions, reported in the literature, was 63.8 (range, 45–79) minutes (Tarsitano et al., 2016).

However, our recent experience revealed as some limits in terms of soft tissues reconstruction accuracy could exist. In particular, virtual surgical planning of soft tissue resection could be affected by a potential bias: the risk of incorrect determination of the resection margins is a substantial clinical problem (Tarsitano et al., 2017). The decision to extend the margins during the surgical procedure, due to positive frozen sections, can imply that the surgical guides and customized fixation plate cannot be optimally used or are no longer serviceable. The potential discrepancy between planned and actual surgical margins is potentially caused by a lack of 3D information concerning tumour spread in soft tissues derivable from CT imaging. Current 3D virtual planning is regularly based on CT images. With CT imaging, the bony structures are segmented and included in the 3D virtual plan.

However, because of the inherent properties of the acquisition device, MRI is preferable, to obtain more detailed soft tissue as well as tumour expansion and invasion information (tumour delineation) (Kraeima et al., 2018). Combining both tumour expansion and invasion information as derived from MRI with the corresponding bone anatomy from the CT provides essential decision-making information concerning the degraded bony tissue and thereby the localisation of resection margins. By using multimodality image staging and tumour delineation, the oncologic margins can be potentially included in the 3D virtual planning.

This method significantly reduces the risk of inaccuracy in terms of soft tissues reconstruction planning. In fact, in our experience, it was never necessary to revert to the conventional surgical approach during surgery or modify the resection planning.

Another concern that we encountered during the use of the SPOG was the potential risk to have an incorrect positioning due to the rotation of the guide around the longitudinal axis of the leg. Although the SPOG has two customized flanges embracing the leg, an estimated rotational error, ranging between 1 and 2 mm, has been observed in our case series. However, this kind of error did not appear to have a clinical impact on the accuracy of the guide in terms of perforator vessel identification and skin paddle's shape harvesting.

Finally, regarding the anatomical pattern of perforator vessels identified on CTA, we classified the vessels of the 84 legs studied into high, medium, and low perforators. The perforator vessels distribution revealed as the majority of the vessels (approximately 40% of the total) were localized in the inferior portion of the leg (between 10 and 15 cm from the external malleolus). The remaining vessels were recorded as medium perforators (between 15 and 20 cm from the external malleolus) and high perforators (between 20 and 25 cm from the external malleolus).

To the best of our knowledge, no prior “in vivo” study has developed such a classification. However, although our innovations are useful in terms of composite reconstruction, preoperative soft tissues planning of both the resected region and the donor site remains challenging and needs further technological improvements.

5. Conclusion

CTA was useful for assessing and virtually simulating mandibular reconstruction using an osteomyocutaneous microvascular fibular free flap. Intra-operatively, the SPOG is a useful tool to identify the soft tissue to be harvested. However, pre-operative soft tissue virtual resection planning remains challenging. A multicentre study is required to explore whether use of our SPOG reproducibly aids reconstruction of intra-oral and cutaneous soft tissues.

Funding sources

This research did not receive any specific grant from funding agencies in the public, commercial, or not-for-profit sectors.

Sources of support

None.

Acknowledgements

The authors thank Mr. Andrea Sandi for his precious and valuable support in virtual planning. We thanks Sintac Biomedical Engineering (Trento, Italy) for customized guides and plates manufacturing.

References

Battaglia S, Maiolo V, Savastio G, Zompatori M, Contedini F, Antoniazzi E, et al: Osteomyocutaneous fibular flap harvesting: computer-assisted planning of perforator vessels using Computed Tomographic Angiography scan and cutting guide. J Craniomaxillofac Surg 45(10): 1681–1686, 2017

Cordeiro PG, Disa JJ, Hidalgo DA, Hu QY: Reconstruction of the mandible with osseous free flaps: a 10-year experience with 150 consecutive patients. Plast Reconstr Surg 104(5): 1314–1320, 1999

Garvey PB, Chang EI, Selber JC, Skoracki RJ, Madewell JE, Liu J, et al: A prospective study of preoperative computed tomographic angiographic mapping of free fibula osteocutaneous flaps for head and neck reconstruction. Plast Reconstr Surg 130(4): 541e–549e, 2012

Hölzle F, Ristow O, Rau A, Mücke T, Loeffelbein DJ, Mitchell DA, et al: Evaluation of the vessels of the lower leg before microsurgical fibular transfer. Part I: anatomical variations in the arteries of the lower leg. Br J Oral Maxillofac Surg 49(4): 2704, 2011

Kraeima J, Schepers RH, van Ooijen PM, Steenbakkers RJ, Roodenburg JL, Witjes MJ: Integration of oncologic margins in three-dimensional virtual planning for head and neck surgery, including a validation of the software pathway. J Craniomaxillofac Surg 43(8): 1374–1379, 2015

Kraeima J, Dorgelo B, Gulbitti HA, Steenbakkers RJHM, Schepman KP, Roodenburg JLN, et al: Multi-modality 3D mandibular resection planning in head and neck cancer using CT and MRI data fusion: a clinical series. Oral Oncol 81: 22–28, 2018

Kumar BP, Venkatesh V, Kumar KA, Yadav BY, Mohan SR: Mandibular reconstruction: overview. J Maxillofac Oral Surg 15(4): 425–441, 2016

Leiggener C, Messo E, Thor A, Zeilhofer HF, Hirsc JM: A selective laser sintering guide for transferring a virtual plan to real time surgery in composite mandibular reconstruction with free fibula osseous flaps. Int J Oral Maxillofac Surg 38: 187–192, 2009

Ribuffo D, Atzeni M, Saba L, Guerra M, Mallarini G, Proto EB, et al: Clinical study of peroneal artery perforators with computed tomographic angiography: implications for fibular flap harvest. Surg Radiol Anat 32(4): 329–334, 2010

Tarsitano A, Mazzoni S, Cipriani R, Scotti R, Marchetti C, Ciocca L: The CAD-CAM technique for mandibular reconstruction: an 18 patients oncological case-series. J Craniomaxillofac Surg 42(7): 1460–1464, 2014

Tarsitano A, Ciocca L, Cipriani R, Scotti R, Marchetti C: Mandibular reconstruction using fibula free flap harvested using a customised cutting guide: how we do it. Acta Otorhinolaryngol Ital 35(3): 198–201, 2015

Tarsitano A, Battaglia S, Crimi S, Ciocca L, Scotti R, Marchetti C: Is a computer-assisted design and computer-assisted manufacturing method for mandibular reconstruction economically viable? J Craniomaxillofac Surg 44(7): 795–799, 2016

Tarsitano A, Ricotta F, Baldino G, Badiali G, Pizzigallo A, Ramieri V, et al: Navigation-guided resection of maxillary tumors: the accuracy of computer-assisted surgery in terms of control of resection margins - a feasibility study. J Craniomaxillofac Surg 45(12): 2109–2114, 2017

Tarsitano A, Battaglia S, Ricotta F, Bortolani B, Cercenelli L, Marcelli E, et al: Accuracy of CAD/CAM mandibular reconstruction: a three-dimensional, fully virtual outcome evaluation method. J Craniomaxillofac Surg 46(7): 1121–1125, 2018

Wilde F, Hanken H, Probst F, Schramm A, Heiland M, Cornelius CP: Multicenter study on the use of patient-specific CAD/CAM reconstruction plates for mandibular reconstruction. Int J Comput Assist Radiol Surg, https://doi.org/10.1007/s11548-015-1193-22015